ELSEVIER

International Journal of Heat and Fluid Flow 21 (2000) 207–212

International Journal of HEAT AND FLUID FLOW

www.elsevier.com/locate/ijhff

Effects of viscosity of fluids on centrifugal pump performance and flow pattern in the impeller

Wen-Guang Li

Hydraulic Machinery Division, Gansu University of Technology, Lanzhou 730050, People's Republic of China

Received 22 May 1999; accepted 17 August 1999

Abstract

Centrifugal pump performances are tested using water and viscous oil as working fluids whose kinematic viscosities are 1 and 48 mm^2/s, respectively, the flows in the centrifugal pump impeller are also measured accurately by using a two-dimensional laser Doppler velocimeter (LDV) in best efficiency and part-loading points, while the pump is handling two kinds of working fluids. The effects of the viscosity on the performance and flow pattern within the impeller are established based on the experimental results. The high viscosity results in rapid increases in the disc friction losses over outsides of the impeller shroud and hub as well as the hydraulic losses in flow channels of the pump. The flow patterns near the impeller outlet are little affected by the viscosity of the fluids, but those near the impeller inlet are greatly affected by the viscosity. There is a wide wake near the blade suction side of the centrifugal pump impeller. The flow pattern is essentially different from the well-known jet/wake model.

Keywords: Fluid; Viscosity; Centrifugal pump; Impeller; Performance

1. Introduction

More researchers have paid attention to the water flow in impellers of centrifugal pumps since the 1950s. Acosta (1954) first examined the water flow in two-dimensional centrifugal pump impellers by using static piezometer taps. Acosta and Bowerman (1957) measured flows of water in five centrifugal pump impellers by using static piezometer taps in the blade surfaces and simple impact probes in the impeller passages. The results show that the relative velocity profile near the suction side of the blade progressively deteriorates from the inner to the outer radial stations. Howard and Kitter (1975) obtained the passage velocities in a radial impeller with closed and semi-open configurations by using a miniature cylindrical hot-film probe. The results show that the primary flow pattern was stable with no tendency toward separation of the suction side boundary layer even near the passage exit. The closed impeller had a secondary flow pattern, which progressed from a single vortex at entry to a vortex near each of the hub and shroud surfaces. The semi-open impeller had a secondary flow pattern, which was a single vortex filling the passage. Murakami et al. (1980) measured the velocity and pressure distributions in the impeller passages of centrifugal pumps by using the cylindrical yaw probe rotating with the impeller. Two impellers with three and seven blades, respectively, were employed to check the effects of the number of the blades. In the seven-blade impeller, the velocity distributions are similar to the potential flow near the inlet of the impeller passage, but the distributions are deformed considerably by a secondary flow developed in passage near the exit of the impeller. In the three-blade impeller, the deformation of velocity distributions is extreme. Hamkins and Flack (1986), Miner et al. (1989) and Flack et al. (1987, 1992) performed turbulence measurements in closed and semi-open impeller, which can orbit in a volute synchronously by using a laser Doppler velocimeter (LDV). From the results, the blade-to-blade velocity profiles were more uniform in the closed impeller than semi-open impeller; the velocity profiles were also more uniform near the exit of the impellers than for small radii; the highest turbulence levels were measured for large radii. Abramian and Howard (1994) conducted an experimental investigation of the steady and unsteady relative flow in a model centrifugal impeller passage by using LDV. The results show that the mean flow within the impeller passage, without the volute in place, is affected by a combined interaction between a secondary vortex, initiated at inlet, and a relative eddy, which dominates the flow at the exit. The combined effects result in a pressure side flow separation under off-design operating condition. Due to the strong effects of the relative eddy, the separation flow reattaches to the pressure side, resulting in a uniform exit through flow, free from wake and distortion. A highly loaded design results in a flow field qualitatively similar to potential flow. Li and Hu (1996) mapped the time-averaged turbulent flow in a centrifugal pump impeller by using LDV. Even though the impeller tip speed is 14.1 m/s, the

E-mail address: liuf@gsut.edu.cn (W.-G. Li).

0142-727X/00/$ - see front matter
PII: S0142-727X(99)00078-8

well-known jet/wake flow pattern did not appear in the impeller flow field. The results mentioned are all obtained while using water as working fluid.

The flow pattern of viscous oil in a semi-open impeller of centrifugal pump has been visualized using the tuft method (Aoki et al., 1985). So far we have little knowledge of the flow of viscous oil in a centrifugal pump impeller.

In this paper, centrifugal pump performances are tested by using water and viscous oil as working fluids whose kinematic viscosity are 1 and 48 mm^2/s, respectively, the flows in the centrifugal pump impeller are also measured accurately by using a two-dimensional LDV in best efficiency and part-loading points as the pump handling two kind of the working fluids. The effects of the viscosity on the performance and flow pattern within the impeller are investigated based on the experimental results.

2. Experimental facility

2.1. Test rig

A special centrifugal pump test rig, shown in Fig. 1, was used to test the pump performance and to measure the flow within the pump impeller when the pump was pumping viscous oil or water. The pump tested is driven by a three-phase AC electric motor, whose rated power is 4.4 kW and speed is 1440 rev/min. The pipe of the rig is made of plastics and its inside diameter is 52 mm. The net volume of the tank is 0.75 m^3 and two rows of cooling pipe are installed in it. A thermometer near outlet of the tank monitors the temperature of oil in the tank, and a gate valve mounted in the discharge pipe controls the operating conditions of the pump. Li (1996) and Li and Hu (1996) have given more information on the rig.

2.2. Performance test method

The pump suction pressure is measured by a differential mercury gage and its discharge pressure is measured by a pressure gage. The capacity of the pump is measured by a turbine or nozzle flow meter. Torque meter measures the shaft torque and speed of the pump. By means of a rotary viscosity meter the viscosity of oil can be given. The density of oil is checked using a floating glass tube density meter.

2.3. Impeller geometry and probe position

The tested centrifugal pump is a single-stage, end suction pump, its design capacity is 25 m^3/h, head is 8 m and speed is 1450 rev/min. The blade outlet and wrapping angles of the impeller are 20° and 140°, respectively. The shroud of the impeller made of metal is machined, then is replaced by a plexiglas plate. A rectangular glass window is mounted on the volute wall located in section IV, shown in Fig. 2.

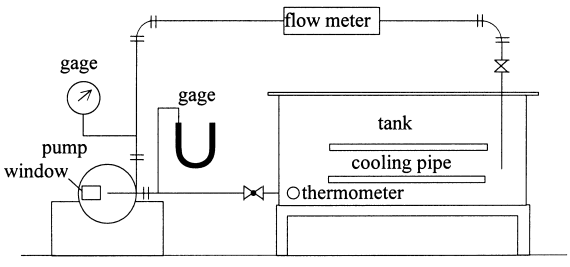

Fig. 1. Centrifugal pump test rig.

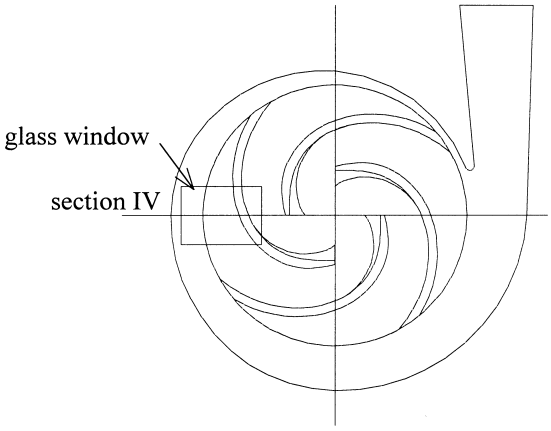

Fig. 2. Impeller and volute configurations.

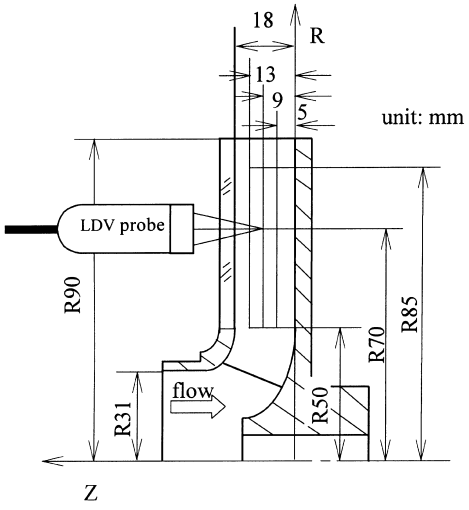

Fig. 3. Probe positions in impeller.

The flow measurements of the viscous oil and water are conducted in section IV of the volute. The LDV probe positions in Z and R directions are shown in Fig. 3. The positions in peripheral θ direction are calculated automatically by a shaft encoder mounted at the end of the motor shaft according to number of sampling and sector as well as window chosen per revolution.

2.4. Working fluid

Working fluids are the special transparent viscous oil refined from crude oils and tap water, respectively. They are Newtonian fluids verified by using the rotary viscosity meter. The density and the kinematic viscosity of the oil are 851 kg/m^3 and 48 mm^2/s, respectively, at 20°C. Fig. 4 is the viscosity–temperature curve of the oil. The density and the kinematic viscosity of the tap water are 1000 kg/m^3 and 1 mm^2/s, respectively, at 20°C. First, the centrifugal pump performance and flow fields in the impeller were measured using the tap water as a working fluid. Then the performance and flow fields were measured again using the viscous oil as a working fluid. However, when the viscous oil was pumping in LDV measurements for 2 or 3 h, the temperature of the oil would be rising due to high friction losses between the oil and flow channel walls. Thus, cooling water would be flowing in the

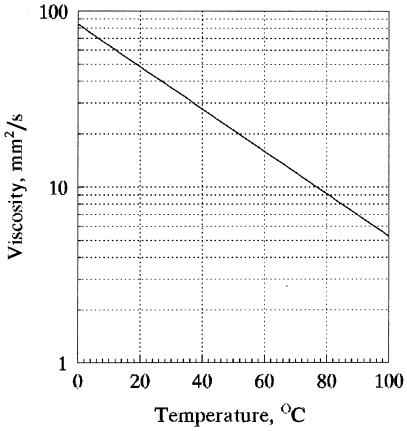

Fig. 4. Viscosity–temperature curve of oil.

cooling pipe installed in the oil tank to maintain the temperature in a constant level.

2.5. Velocimeter

Velocimeter is a four-beam, two-color (blue and green), and back-scattered LDV system (TSI) which can measure two-dimensional flow fields in a point-by-point mode. A shaft encoder rotating with the pump shaft is mounted at the end of the motor shaft. The encoder records the impeller angular position. The optical probe of the LDV is moved to an expected location using a manual three-coordinate transverse system, then a personal computer performs sampling, processing for data etc.

2.6. Uncertainty

The uncertainties in head, capacity, torque, speed and efficiency are 0.47%, 0.5%, 0.3%, 1% and 1.15%, respectively. The uncertainty of the LDV in velocity is 1.8% and the uncertainty in probe position is 5.0%, so the total uncertainty of LDV is 5.3%.

3. Results and discussions

3.1. Effects of viscosity on performance

Fig. 5 shows the centrifugal pump performances while the pump handles water with kinematic viscosity 1 mm^2/s and viscous oil with viscosity 48 mm^2/s at rotating speed $n = 1485$ rev/min at 20°C. The best efficiency points (BEP) located at $Q_{BEP} = 5.93$ and 5.86 l/s, corresponding to the best efficiencies are 56.65% and 47.2%, respectively. The LDV measurements are conducted in the two operation conditions marked △ in the head curve, two are the BEPs, the others are the part-load points (PLP) which are located at $Q = 0.58Q_{BEP}$, respectively.

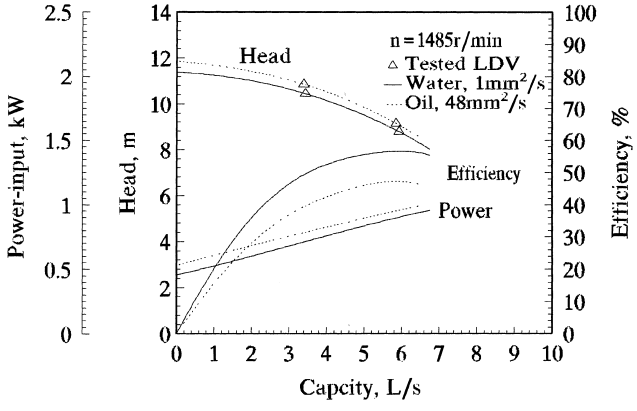

Fig. 5. Pump performance for different viscosities.

The pump head and power-input for the pump handling oil are higher than those for handling water, but the efficiency for handling oil is lower than that for handling water as shown in Fig. 5. The pump efficiency dropping while pumping the oil results from the fact that the disc friction losses over the outsides of the impeller shroud and hub as well as the hydraulic losses in flow channel of pump are increasing rapidly. In order to verify this fact, additional experimental works have been done for testing the impeller disc friction loss as the oil viscosity increases. Suppose that the disc loss does not depend on pump work condition, so the test data in shut-off condition can be used to estimate the disc loss. The losses in pump involve two parts, one is the disc friction loss and the other is the vortex loss due to the interaction between impeller and volute in the shut-off condition. The disc friction loss can be evaluated by using Pfleiderer's (1955) famous formula, pumping water. The vortex loss for pumping water will be estimated through subtracting the disc friction loss from the power-input in shut-off condition. This vortex loss is assumed to maintain the same value while pumping the oil, therefore the disc friction losses will be estimated through subtracting the vortex loss from the power-input in shut-off condition for higher kinematic viscosity fluid. From the additional experimental data, the disc friction losses relate to the kinematic viscosity of the working fluids as follows:

$$\frac{P_{ds}}{P} = 0.098 \times 1.0109^{v}, \tag{1}$$

where P_{ds}, P and v represent the disc friction loss, power-input, and the kinematic viscosity, respectively. This equation is a regression equation only for the available data in which the kinematic viscosity of fluid is <61 mm^2/s.

Meanwhile, the hydraulic loss for pumping oil increases to 34% from 28% for handling the water. The hydraulic loss is calculated through mechanical and volumetric losses as well as total efficiency of the pump based on the performance and LDV results. The disc loss is considered as the main component of the mechanical loss being calculated. The pump efficiency can be written as $\eta = \eta_m \eta_V \eta_h$ in the BEP. The hydraulic loss is $\varepsilon = 1 - \eta_h$. The pump efficiency η and mechanical efficiency η_m have been given in the performance test. The volumetric efficiency η_V can be calculated based on the wearing ring geometry parameters and pressure differential across the clearance of the ring. The pressure differential depends on the impeller inlet and outlet static pressures. The pressure in the pump inlet has been measured in the performance test. The outlet static pressure is estimated through subtracting the absolute velocity head of fluid in the pump volute from the total head of the pump. The absolute velocity has been mapped by the LDV at the pump impeller outlet. Hence the volumetric efficiency η_V can be worked out. More details of the calculation procedure can be found in Li (1996).

The pump head increasing while the pump handles oil is due to the slip factor near the impeller outlet becoming less. This phenomenon will be illustrated in Table 1 and Fig. 10.

In order to illustrate this fact, five streamlines are chosen, as shown in Fig. 6. In the absolute coordinate system, which is fixed in the pump casing, specific absolute energy of fluid particle (i.e. specific energy) is

Table 1
Specific energy and head

	PLP		BEP	
	V_uU/U_2^2	H (m)	V_uU/U_2^2	H (m)
Water	0.790	10.95	0.694	9.22
Oil	0.847	11.39	0.755	9.59

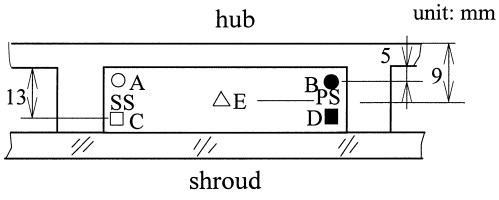

Fig. 6. Five streamlines chosen.

$$\frac{p}{\rho}+\frac{V^2}{2}=\frac{p^*}{\rho}+V_uU, \tag{2}$$

where p, ρ, V, V_u, p^* and U represent fluid static pressure, density, absolute velocities, its peripheral component and stagnation pressure in a relative coordinate system, which is fixed in the impeller, impeller peripheral speed, respectively. For ideal fluids, p^*/ρ in each streamline is the same, so that the specific energy only depends on V_uU. However, for real fluids the specific energy depends on both p^*/ρ and V_uU, but V_uU still is the main part of the specific energy, then V_uU can represent the specific energy of fluid particles in a streamline approximately. On other hand, the specific energy can demonstrate the fluid slip situation. If the specific energy near the impeller outlet is large, the slip factor will be small, otherwise large.

The arithmetic average values of the specific energy in the five streamlines at $R = 85$ mm location measured as well as the pump head H in the same working conditions are shown in Table 1. V_u values have been obtained from LDV measurements, and U_2 represents the impeller tip peripheral speed. The specific energy while the pump handles oil is higher than that when it handles the water in both BEP and PLP, hence the slip while handling oil is less than that while handling water. Physically, the higher viscosity of the oil allows a weaker relative circulation within impeller flow channel than that of the water. The heads measured show the same trend as the specific energy while the viscosity of the working fluids is increasing. Thus the LDV results relate to the pump performance very well.

3.2. Effects of viscosity on flow pattern

Relative velocity profile. Fig. 7 shows the relative velocity profiles of the water and the oil between blade-to-blade in middle span, i.e. $Z = 9$ mm stream surface in BEP, where θ, θ_B and W represent peripheral angle, center angle between blade pressure and suction sides at same radius, as well as relative velocity of the fluids, respectively.

Fig. 7(a) shows the relative velocity profiles of the water in BEP at $R = 50$ and 85 mm. From the figure, the velocity near blade suction side (SS) is much higher than that near blade pressure side (PS) at $R = 50$ mm, the variation of the profile is similar to that predicted by the potential flow theory. However, the velocity near SS is obviously lower than that near PS at $R = 85$ mm, so that the variation is opposite to that predicted by the potential flow theory.

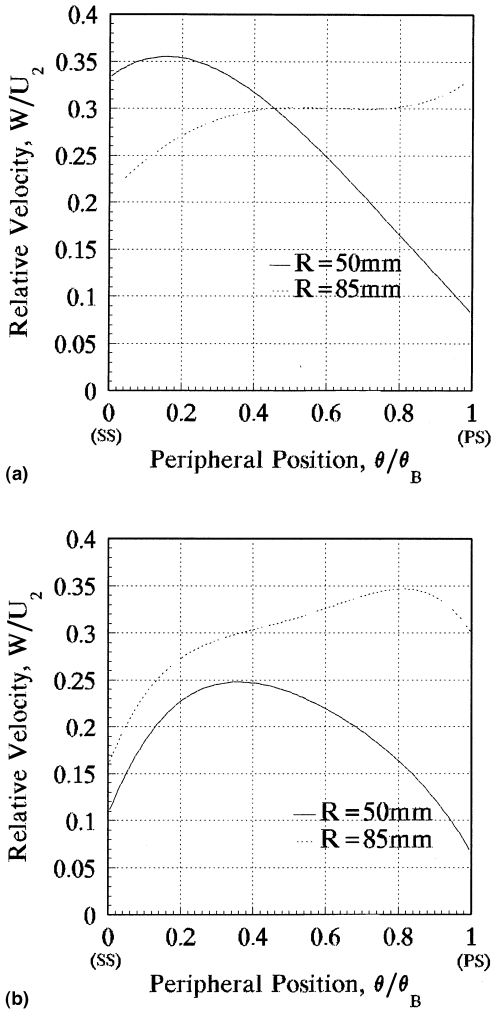

Fig. 7. Relative velocity profiles in BEP.

Fig. 7(b) shows the relative velocity profiles of the oil in BEP at $R = 50$ and 85 mm. The velocity near SS is almost equal to that near PS at $R = 50$ mm, the variation trend of the profile is not similar to that predicted by the potential flow theory. The maximum of the velocity located at 36% of width along θ direction from SS at $R = 50$ mm. The velocity near SS is also lower than that near PS at $R = 85$ mm. The variations of the profiles are opposite to those predicted by the potential flow theory at both $R = 50$ and $R = 85$ mm locations.

Fig. 8(a) shows the relative velocity profiles of the water in PLP at $R = 50$ and 85 mm. The velocity near SS is a little higher than that near PS at $R = 50$ mm, and the velocity near SS is also much lower than that near PS at $R = 85$ mm, so that the variations are opposite to that predicted by the potential flow theory. The maximum of the velocity is located at about 40% of width along θ direction from SS at $R = 50$ mm. The variations of the profiles are opposite to that predicted by the potential flow theory at both $R = 50$ and $R = 85$ mm locations.

Fig. 8(b) shows the relative velocity profiles of the oil in PLP at $R = 50$ and 85 mm. The velocity near SS is lower than that near PS at $R = 50$ mm, the variation of the profile is not similar to that predicted by the potential flow theory. The maximum of the velocity is located at about 44% of width

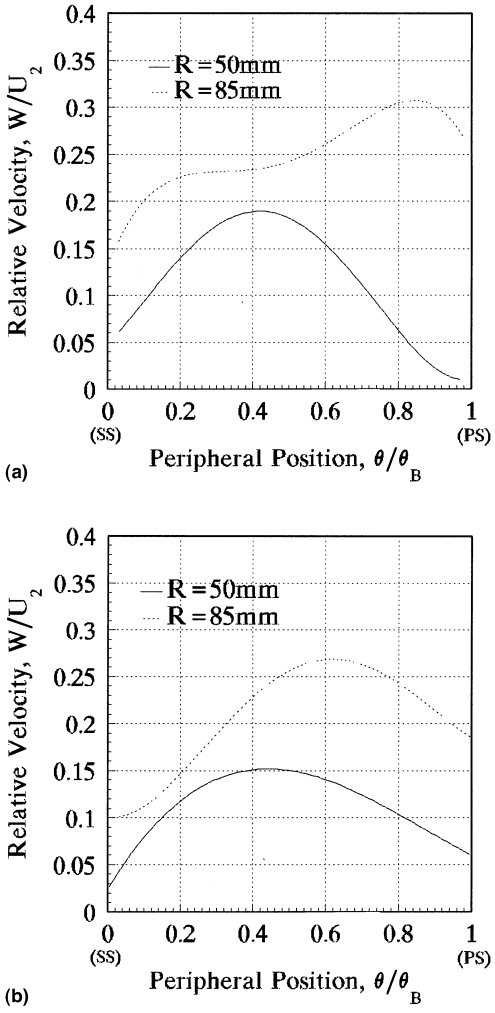

Fig. 8. Relative velocity profiles in PLP.

along θ direction from SS at $R = 50$ mm. The velocity near SS is also lower than that near PS at $R = 85$ mm. The variations of the profiles are opposite to that predicted by the potential flow theory at both $R = 50$ and $R = 85$ mm locations.

In both BEP and PLP, the flow patterns corresponding to the oil and the water are almost the same near the impeller outlet. As shown in the figures the relative velocities near SS are much lower than those near PS at $R = 85$ mm, so a wake will exist in SS near the impeller outlet. The relative velocity, i.e. momentum of the oil or water in the boundary layer near SS is slow or small in the relative reference coordinate system in BEP and PLP. This means that the oil or water in the boundary layer near SS has a low kinetic energy in the relative coordinate system due to the pressure on SS being lower compared to that on PS at same radial position. Hence, the boundary layer with slower relative velocity near SS essentially is a wake. The flow outside the wake is the so-called 'primary flow'. A shear layer between the wake and the primary flow does not exist. Thus the primary flow near PS is not a jet; therefore, the flow pattern in the impeller measured does not yield the well-known jet/wake pattern commonly found in radial or forward-curved blade of impeller of centrifugal compressor or blower. This so-called 'primary flow/wake' pattern is essentially different from the jet/wake pattern. The wake near SS is characterized by lower relative velocity compared with its surrounding flow, so the wake width should be estimated based on the relative velocity distribution between blade-to-blade. It is proposed that the flow region near SS in which the relative velocity of the viscous oil or water is lower than the averaged velocity measured by LDV is the wake in this paper. The wake covers 30–50% of the channel width along θ direction approximately.

In BEP, the flow pattern for pumping oil is different from that for pumping water near the SS only. The relative velocity for handling oil, which is shown in Fig. 9(a), is lower than that for pumping water near the SS, which is shown in Fig. 9(b). This results in the impeller transferring more energy to oil than that to water in the same work condition near the SS. This means that the flow slip for pumping oil is less than that for pumping water.

In PLP, the relative velocity for handling oil, which is shown in Fig. 10(a) is also lower than that as pumping water near the SS, which is shown in Fig. 10(b). Two separated flow zones will be found, one is near the SS and the other near the PS in Fig. 10(a), only one separated flow zone will be found near SS in Fig. 10(b). Therefore, the high viscosity would suppress the flow separation from the PS. Physically, the high viscosity would make the angle of attack and the local blade hydrodynamic loading vary considerably, this needs to be studied further.

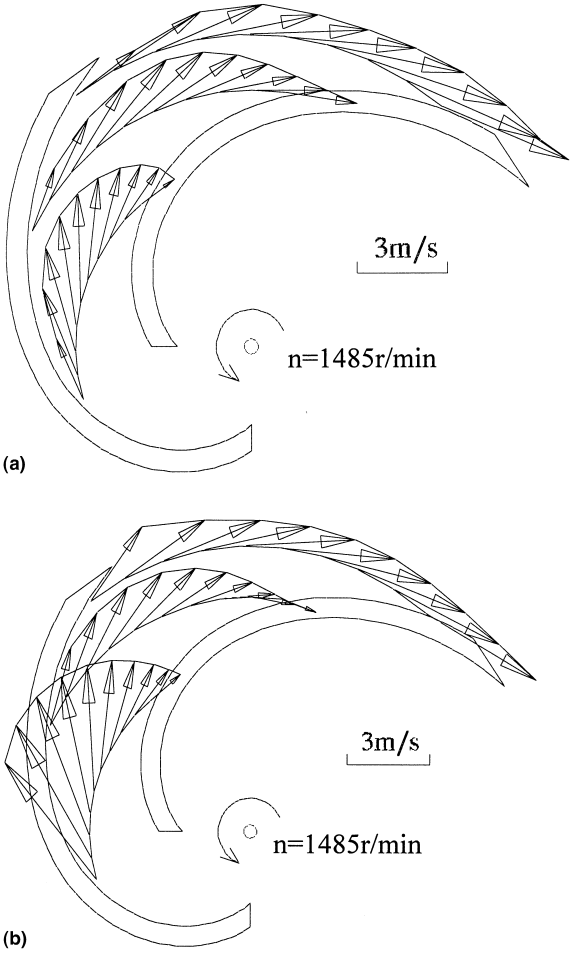

Fig. 9. Relative velocity vectors in BEP.

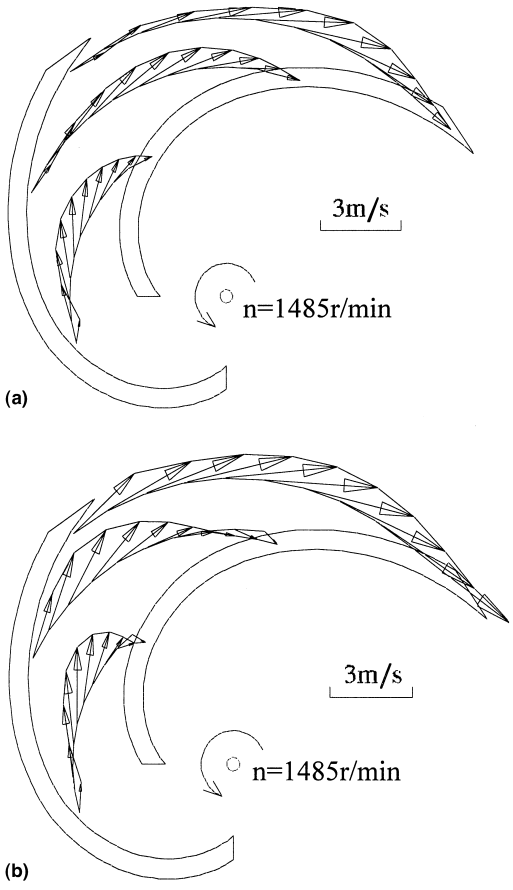

Fig. 10. Relative velocity vectors in PLP.

4. Conclusions

(1) The reason why a centrifugal pump's performance goes down when the pump handles high viscosity working fluids, is that high viscosity results in a rapid increase in the disc friction losses over outsides of the impeller shroud and hub as well as in hydraulic losses in flow channels of the pump.

(2) The flow patterns near the impeller outlet are less affected by the viscosity of the fluids in best efficiency and part-loading points, but the flow patterns near the impeller inlet are greatly affected by the viscosity.

(3) There is a wide wake near the blade suction side of the centrifugal pump impeller, there is not a jet near the blade pressure side, and the flow pattern is essentially different from the well-known jet/wake model.

References

Abramian, M., Howard, J.H.G., 1994. Experimental investigation of the steady and unsteady relative flow in a model centrifugal impeller passage. ASME J. Turbomachinery 116 (2), 269–279.

Acosta, A.J., 1954. An experimental and theoretical investigation of two-dimensional centrifugal pump impellers. Trans ASME 76, 749–763.

Acosta, A.J., Bowerman, R.D., 1957. An experimental study of centrifugal pump impellers. Trans ASME 79, 1821–1839.

Aoki, K., Yamamoto, T., Ohta, H., 1985. Study on centrifugal pump for high viscosity liquids. Trans JSME (B) 51 (468), 2753–2758.

Flack, R.D., Hamkins, C.P., Brady, D.R., 1987. Laser velocimeter turbulence measurements in shrouded and unshrouded radial flow pump impellers. Int. J. Heat and Fluid Flow 8 (1), 16–25.

Flack, R.D., Miner, S.M., Beaudoin, R.J., 1992. Turbulence measurements in a centrifugal pump with a synchronously orbiting impeller. ASME J. Turbomachinery 114 (2), 350–359.

Hamkins, C.P., Flack, R.D., 1986. Laser velocimeter measurements in shrouded and unshrouded radial flow pump impellers. ASME J. Turbomachinery 109 (1), 70–78.

Howard, J.H.D., Kitter, R.D., 1975. Measured passage velocities ina rafial impeller with shrouded and unshrouded configurations. ASME J. Eng. Power 97 (2), 207–213.

Li, W.-G., 1996. LDV measurements and calculations of internal flows in the volute and impellers of centrifugal oil pump. Ph.D. Dissertation, Petroleum University, Beijing, pp. 76–116.

Li, W.-G., Hu, Z.-M., 1996. Time-averaged turbulent flow LDV measurements in a centrifugal pump impeller. Pump Technol. 4, 18–29.

Miner, S.M., Beaudoin, R.J., Flack, R.D., 1989. Laser velocimeter measurements in centrifugal flow pump. ASME J. Turbomachinery 111 (3), 205–212.

Murakami, M., Kikuyama, K., Asakura, E., 1980. Velocity and pressure distributions in the impeller passages of centrifugal pumps. ASME J. Fluids Eng. 102 (4), 420–426.

Pfleiderer, C. (Ed.), 1955. Die Kreisepumpen. Springer, Berlin, p. 99.